Analytica Chimica Acta 925 (2016) 70–81

Contents lists available at ScienceDirect

Analytica Chimica Acta

journal homepage: www.elsevier.com/locate/aca

Fabrication of interdigitated high-performance zinc oxide nanowire modified electrodes for glucose sensing

R. Haarindraprasad [a], Uda Hashim [a, *], Subash C.B. Gopinath [a, b], Veeradasan Perumal [a], Wei-Wen Liu [a], S.R. Balakrishnan [a]

[a] Biomedical Nano Diagnostics Research Group, Institute of Nano Electronic Engineering (INEE), Universiti Malaysia Perlis (UniMAP), 01000 Kangar, Perlis, Malaysia
[b] School of Bioprocess Engineering, Universiti Malaysia Perlis (UniMAP), 02600 Arau, Perlis, Malaysia

HIGHLIGHTS

- ZnO nanowire (NW) modified Interdigitated electrode (IDE) to monitor the level of glucose is fabricated using silver.
- Amendment of ZnO-based thin film and NW were done.
- ZnO thin films that was annealed yielded a good quality crystallite sized, 50, 100 and 110 nm.
- A flower-model NW was obtained with the lowest diameter of 21 nm.
- Designed IDE was shown to have the detection limit as low as 0.03 mg/dL of glucose with a fast response time of 3 s.

GRAPHICAL ABSTRACT

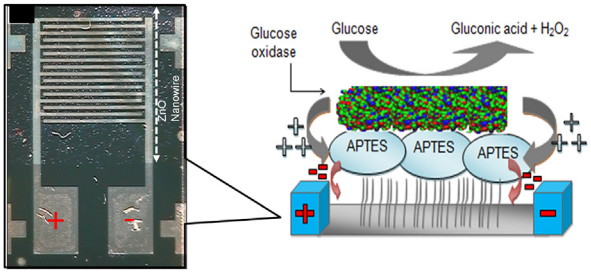

ARTICLE INFO

Article history:
Received 30 July 2015
Received in revised form
16 March 2016
Accepted 15 April 2016
Available online 26 April 2016

Keywords:
Interdigitated electrode
ZnO nanowire
Glucose
Biosensor
Sol–gel

ABSTRACT

Diabetes is a metabolic disease with a prolonged elevated level of glucose in the blood leads to long-term complications and increases the chances for cardiovascular diseases. The present study describes the fabrication of a ZnO nanowire (NW)-modified interdigitated electrode (IDE) to monitor the level of blood glucose. A silver IDE was generated by wet etching-assisted conventional lithography, with a gap between adjacent electrodes of 98.80 μm. The ZnO-based thin films and NWs were amended by sol–gel and hydrothermal routes. High-quality crystalline and c-axis orientated ZnO thin films were observed by XRD analyses. The ZnO thin film was annealed for 1, 3 and 5 h, yielding a good-quality crystallite with sizes of 50, 100 and 110 nm, and the band gaps were measured as 3.26, 3.20 and 3.17 eV, respectively. Furthermore, a flower-modeled NW was obtained with the lowest diameter of 21 nm. Our designed ZnO NW-modified IDE was shown to have a detection limit as low as 0.03 mg/dL (correlation coefficient = 0.98952) of glucose with a low response time of 3 s, perform better than commercial glucose meter, suitable to instantly monitor the glucose level of diabetes patients. This study demonstrated the high performance of NW-mediated IDEs for glucose sensing as alternative to current glucose sensors.

* Corresponding author.
E-mail address: uda@unimap.edu.my (U. Hashim).

http://dx.doi.org/10.1016/j.aca.2016.04.030
0003-2670/

1. Introduction

The World Health Organization (WHO) has reported that diabetes is a chronic disease, affecting 347 million people worldwide [1]. As a consequence, awareness of diabetes has become an important issue from a clinical viewpoint to prevent this metabolic disease and to have healthier lives. In addition to improved awareness, fast detection of the blood glucose level is another key factor for reducing complications with diabetes by taking medication earlier. Therefore, designing a portable and less expensive glucose biosensor has become a goal for 'bedside analysis.' Previously, the development of glucose biosensors has relied on electrochemistry [2], chemiluminescence [3], surface-enhanced Raman scattering [4], and electrochemical [5,6] and transistor sensors [7]. Enzyme-based electrochemical sensing was reported for straightforward, relatively low-cost, and more sensitive detection of glucose [8,9]. Recently, Luo et al. (2013) developed a surface acoustic wave (SAW) device for glucose sensing, which has extraordinary characteristics including higher sensitivity, higher selectivity, a fast response, and portability. However, the major drawback of the SAW device is that its fabrication is complicated, requiring the development of an alternate, simplified sensing method such as an interdigitated electrode (IDE). The IDEs generated in the past have been composed of multiple adjacent electrodes and can act as capacitive sensors [10]. Moreover, IDEs embedded in a suitable thin film facilitate better performance with surface functionalization for biosensing applications [11]. In this study, with a view to generate a novel sensing system, distinct from previous works, a zinc oxide (ZnO) thin film was embedded with an IDE and investigated for glucose sensing as a novel application.

ZnO has become a promising material among other oxide materials for its development in various applications due to its extraordinary electrical and optical properties [12–16]. Moreover, an easy and simplified route for synthesizing ZnO NWs has made it an attractive and essential material for the development of high-performance biosensors. ZnO NWs are widely considered to be a preferable option for use as transducers in biosensors due to their increased surface area to volume ratio, which is strongly associated with their elevated sensitivities [17–20]. ZnO NWs also facilitate the specific immobilization of negatively charged proteins, such as glucose oxidase (GOx), which has an isoelectric point of 4.2 (an acidic pH) [21,22]. With the appropriate material, the generation of sensors with promising sensitivity could be a hallmark for high-performance interaction analyses with a wide range of biomolecules, including small molecules [23]. Higher sensitivity with ZnO NWs has been shown through their significantly high electron mobility, which is close to 1000 cm^2/V [24]. Moreover, ZnO materials have a large binding energy (60 meV) and large band gap (3.37 eV) [25,26], which makes the materials more stable.

By applying the above favorable characteristics of ZnO, herein, we demonstrated the fabrication of a ZnO NW-modified IDE as an electrochemical glucose sensor, a novel type of sensing element. ZnO NW-modified IDE can be use in DC current (battery system) which is tailored for bedside analyses. To generate this sensor, a ZnO thin film was prepared using the sol–gel method; the film was coated on a silicon wafer, a straightforward and low-cost route of synthesis with the desired crystallite size range [13,27,28]. The construction and modification process taken to develop the glucose sensor is actually not time consuming compared to other developed glucose sensor. The newly developed sensor which involve Interdigitated electrodes (IDE) system is less complex because it only involve two working electrode system and only one mask compared to other sensor such as FET and ISFET system which involve complex fabrication steps. The fabricated ZnO NW-modified IDE electrochemical glucose biosensor is economical compared to conventional glucose sensor because conventional glucose sensor involve gold pad electrode which is very costly. The fabrication process of the ZnO NW-modified IDE glucose sensor is less complex and also reduces the production cost. Studies shows that zinc oxide material is considered economical globally. The proposed Interdigitated Zinc Oxide Nanowire modified electrode (IDE) sensor contains lot of advantages compared conventional glucose meter, such as the dimensional size of the sensor, simplicity, reliability and economical. We demonstrated the detection of glucose at lower levels, which is highly suitable for diabetes patients, can be feasible for and conducive to glucose monitoring, and has practical and commercial potential.

2. Experimental

2.1. Consumable materials

The ZnO seed solution was prepared using zinc acetate dehydrate [$Zn(CH3COO)_2.2H_2O$] (98%; Sigma–Aldrich, St. Louis, Missouri, USA), which was free of chlorine ions and used as a precursor. Solvents such as 2 methoxyethanol, 2-ME (99.8%; Sigma–Aldrich, J.T. Baker, Center Valley, Pennsylvania, USA) were used without further purification. Monoethanolamine (MEA; 99%; Merck, Kenilworth, New Jersey, USA) was used as a stabilizer. Buffered oxide etchant (BOE; 6:1; J.T. Baker, Center Valley, Pennsylvania, USA), negative photoresist (NR7-6000PY; Futurrex, Franklin, New Jersey, USA) and resist developer (RD6; Futurrex, Franklin, New Jersey, USA) were used for the photolithography. The growth solution was prepared by mixing equal concentrations (25 mM) of zinc nitrate hexahydrate (99%; Sigma Aldrich, St. Louis, Missouri, USA) and hexamethylenetetramine (99%; Merck, Kenilworth, New Jersey, USA) in DI water. (3-Aminopropyl) triethoxysilane, 99% (APTES) and glucose oxidase (GOx) G3660-1CAP were purchased from Sigma Aldrich Sdn. Bhd (Malaysia) and were used for immobilization process. The glucose sample, dextrose monohydrate (DEX) $C_6H_{12}O_6$, H_2O (100%, Malaysia), was purchased from a pharmacy.

2.2. Sample wafer preparation

Silicon p-type samples with an orientation of <100> were cleaned by immersing them in RCA 1 and RCA 2 solutions to eliminate unwanted substances. Next, samples were immersed in BOE solution to remove contaminants such as oxide layers and to improve the hydrophobic character of the samples. Removing the oxide layer is a necessary step in sample preparation to ensure that the ZnO thin film would be coated properly with minimal defects and in a uniform orientation.

2.3. Fabrication of interdigitated electrodes (IDE)

Silver IDE electrode was deposited on the silicon wafer sample with an orientation of <100>, using the traditional wet etching method. Positive photoresist (PR) was coated on the silicon wafer, followed by a soft bake for 90 s. Ultraviolet (UV) light exposure was conducted for 10 s to allow the pattern to be transferred from the IDE mask onto the sample. Next, the sample was developed for 15 s using the RD-6 developer. Then, sample was baked at 110 °C to remove unwanted moisture and to enhance the adhesion between the silver and SiO_2 layers. Finally, the unexposed area was removed using a silver etchant for 23 s and then cleaned with acetone. The time consume for fabricate the IDE sensor is approximately 180 s only. The fabrication process of the IDE electrode which involves photolithography process was conducted at room temperature (23 °C).

2.4. Synthesis of ZnO seed layer

A facile chemical route, the sol–gel method, was used to synthesize the ZnO solution. The solute, solvent and sol stabilizer were used in this sol gel process were zinc acetate powder, 2-methoxyethanol and monoethanolamine (MEA), respectively. The concentration of zinc acetate powder used was 0.2 mol/L, which was dissolved in 20 ml 2-methoxyethanol. Then, the mixture was heated at 60 °C and stirred with a rotational speed of 1000 rpm for 20 min on a hot plate. The molar ratio of zinc acetate to MEA was set at 1:1, and this solution was added to the mix dropwise at constant intervals of 10 min for 2 h. The obtained clear and homogeneous solution was kept at room temperature for 24 h for aging.

2.5. ZnO thin film coating procedure

The prepared ZnO seed solution was coated on SiO_2 using a spin coater. After coating, the sample was preheated at 60 °C for 20 min in order to form nuclei for the crystallization of ZnO thin films. Then, temperature was increased to 150 °C and heated for 10 min; next, the sample was cooled down slowly to 50 °C to avoid cracks or dislocations of the structure on the thin films. Finally, the ZnO thin film was annealed at 200 °C for 1, 3 and 5 h.

2.6. Synthesis of ZnO nanowires (NWs) on IDE using the hydrothermal method

ZnO NWs were synthesized using an aqueous chemical growth method. Hexamethylenetetramine and Zn $(NO_3)_2$ at a concentration of 0.025 mol/L were dissolved in distilled water of 200 ml. Then, the mixture solution was stirred at 1000 rpm for 25 min. The as-prepared ZnO thin film was immersed in the mixture solution for growing the ZnO NWs at 93 °C for 5 h. The annealing process to crystalline the ZnO NW was conducted at 200 °C.

2.7. Characterization of the ZnO NWs

The morphology of the ZnO NWs was characterized under a scanning electron microscope (SEM: JSM-6460). X-ray diffraction (XRD) patterns were obtained from a Rigaku MultiFlex. The absorbance and transmittance of ZnO thin films coated on glass slides were investigated at normal incidence using a UV–visible (UV–VIS) spectrometer (PerkinElmer model Lambda 35). The electrical measurement was conducted at room temperature using the two-point probe technique coupled with a SourceMeter (model Keithley 2400), interfaced to a LabView Leios TMXpert simulator, and a voltage supply ranging from zero to +2 V was used.

2.8. Surface functionalization of ZnO NWs for the immobilization of glucose oxidase (GOx)

Before functionalization by 3-aminopropyltriethoxysilane (APTES), the ZnO NWs were cleaned using ethanol and then dried under N_2 gas. To functionalize the ZnO NWs, the ZnO NWs were immersed in 0.2 μL of a mixture solution containing 2% APTES, 95% DI water, and 3% ethanol. The functionalized ZnO NWs were dried under infrared light emission for 1 h. Finally, the GOx enzyme was prepared as suggested by the manufacturer (1 g was dissolved in 39.2 ml of double-distilled water), and 3.0 μL of the solution was then spotted on the functionalized ZnO NWs and was left for 30 min for the proper immobilization of GOx.

2.9. Dextrose monohydrate and blood sample preparation

The fresh glucose samples, standard dextrose monohydrate (DEX) undergoes serial dilution method to prepare 7 different concentrations of DEX ranging from 0.03 to 30,000 mg/dL. Blood sample was obtained from the volunteers. About 2 ml of patient's blood was collected by venipuncture into a tube containing a mixture of ethylenediaminetetra acetic acid (EDTA) and sodium fluoride in the ratio of 1:2 (W/W). Then 0.1 ml of blood was added into 1.8 ml of sodium sulphate-zinc sulphate reagent in a centrifuge tube, followed by 0.1 ml of 2 N Sodium hydroxide was added and centrifuged at 3000 rpm for 5 min. Further, the centrifuged blood samples were tested and compared with commercial glucose meter and the developed Interdigitated ZnO NW modified electrode sensor.

3. Results and discussion

Diabetes is a human health issue all over the world, causing uncomfortable situations in combination with cardiovascular diseases. To overcome these issues with diabetes and for early alertness in a departure from the conventional laboratory methods, in this present study, a glucose sensor was fabricated by developing a ZnO NW-modified IDE. The synthesized ZnO NW functions as a transducer to monitor the glucose level. The glucose level in a healthy person is in the range of 100–140 mg/dL. The fabrication process for the silver IDE, intended to achieve detection levels better than the above-mentioned glucose level in healthy humans, as shown in Fig. 1A.

3.1. Interdigitated electrode (IDE)

The designed IDE with a uniform pattern and the distance between adjacent electrodes was measured using high-power microscopy (HPM), as shown in Fig. 1B. The measured gap size between adjacent electrodes was 98.80 μm, which was tailored to increase the sensitivity for detecting the dielectric properties of the bio-molecular substances. The diameter of the fabricated individual electrode fingers was 108.72 μm. The sensitivity of the IDE was improved through reducing the gap size of the adjacent electrodes as described by the following formula:

$$C = \varepsilon_0 \varepsilon_r \left(\frac{A}{L}\right) \quad (1)$$

where 'A' represents the area of the electrode, 'L' is the distance between adjacent electrodes and ε_o is the permittivity of free space [29]. Based on the above Equation (1), a smaller distance between adjacent electrodes would yield higher IDE sensitivity. Higher nanogaps in the sensing area on the proposed sensor will cause deterioration of the sensitivity performances. More potential energy is required for the electron to flow between the larger gaps in the sensing area. Hence, smaller gaps between the electrode fingers increase the sensitivity performances of the proposed sensor. The fabricated silver IDEs are coated by the ZnO thin film prior to the ZnO NW formation by the hydrothermal method. A silver electrode is utilized due to its favorable electrical properties and ease of conducting the wet etching photolithography process.

3.2. Synthesis of ZnO NWs

The sizes of the synthesized ZnO NWs on the silver IDE were closely observed by scanning electron microscopy (SEM). The shape and the diameter of the ZnO NWs are clearly illustrated in Fig. 2A–D. The figure shows SEM and FESEM images and displays the highly dense and uniform-sized ZnO NWs with sharp tips. The SEM images show that the long NWs have tips with smaller diameters. The presence of sharp tips is important to entrap tiny bio-

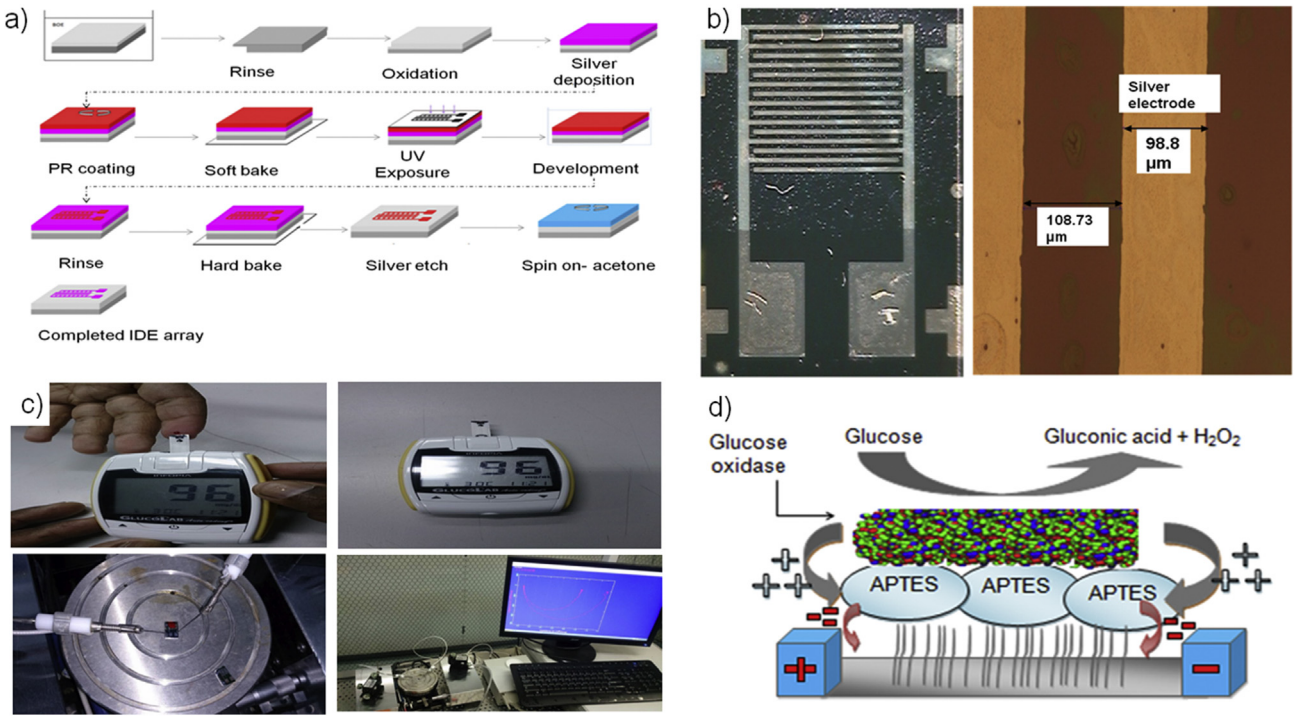

Fig. 1. (a) Process flow fabrication of IDE using conventional photolithography method, (b) high power microscopy (HPM) image of the IDE for spacing measurements. The gap size between the adjacent electrodes was 98.74 µm, and the size of electrode was 108.72 µm. (c) Comparison measurement of well-established glucose biosensor and fabricated Zinc Oxide NW IDE glucose sensor. (d) Diagrammatic illustration of the working mechanism of the Interdigitated high-performance zinc oxide NW-modified electrode for glucose biosensing.

molecular substances. Previously, the sharp tips of ZnO NWs demonstrated extremely high sensitivities as substitutes for carbon nanotubes (CNTs) for future sensing elements [30].

The SEM images indicate that there were variations in the diameters of the NWs when the ZnO thin films were annealed for different lengths of time. However, when the ZnO thin films were annealed for 3 and 5 h, the difference in the diameters of the NWs was not significant. The average diameters of the ZnO NWs for the 3 and 5 h annealing times were measured as approximately 128 nm and 193 nm, respectively (calculated by averaging 200 NWs).

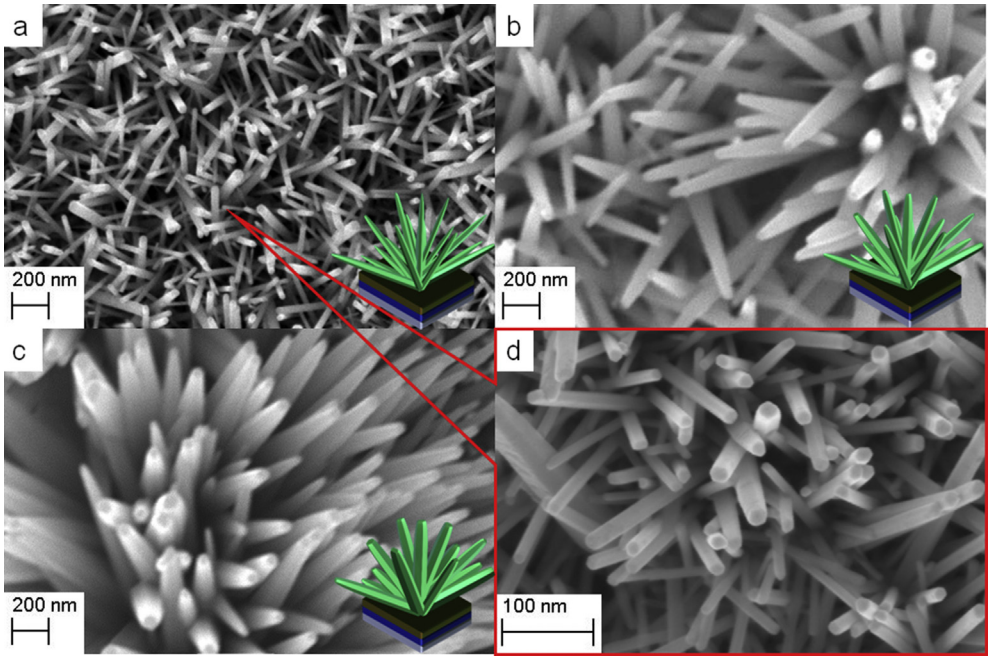

Fig. 2. Visual inspection of the structural shape and size of the synthesized ZnO NWs. SEM images of the ZnO NWs with a magnification of × 20k formed by ZnO thin films that were annealed at different temperatures for (a) 1 h, (b) 3 h, and (c) 5 h (d) FESEM image of the ZnO NWs a with magnification of × 150k annealed for 1 h.

However, the diameters of the ZnO NWs changed drastically when the annealing time was reduced to 1 h. The smallest diameter of the ZnO NWs was determined to be 21 nm, which is excellent for detecting biomolecules due to a high surface area to volume ratio [31]. Thus, the diameters of the ZnO NWs increased with the increasing annealing time of the ZnO thin films. The main reason for this behavior might be due to the increased grain crystal size, which recovers the structural defects on the grain. Initially, the grain crystals of the ZnO thin films contain many voids and vacancies. After treating for a longer annealing time, a recrystallization process occurred, causing repositioning in the lattice structure of the thin film. The recrystallization process, which recovers the voids in the grain crystal, might cause the increase in the grain size. Hence, when the grain size of the thin film is increased, the diameter of the synthesized ZnO NWs is larger by the hydrothermal method. In this study, the ZnO NWs were synthesized using the hydrothermal growth process for 5 h to ensure that the fabricated ZnO NWs were grown uniformly and with the correct orientation compared to the previous studies reported by Xu et al. (2013) [32]. However, in the study of Xu et al. (2013), a ZnO growing process of more than 8 h produced less-uniform and larger-size of ZnO NWs. In addition, a longer growth period for ZnO NWs in aqueous solution leads to non-uniform NWs due to the non-homogenous formation of ZnO NWs [33].

3.3. Formation of ZnO NWs

The following chemical equations describe the chemical reactions involved in the hydrothermal method for forming the ZnO NWs:

$$(CH_2)_6N_4 + 6H_2O \leftrightarrow 6HCHO + 4NH_3 \quad (2a)$$

$$NH_3 + H_2O \leftrightarrow NH_4^+ + OH^- \quad (2b)$$

$$2OH^- + Zn^{2+} \leftrightarrow ZnO(s) + H_2O \quad (2c)$$

Initially, hydroxide ion (OH^-) is produced from the reaction between H_2O and NH_3. The formation of ZnO NWs is completed when OH^- reacts with Zn^{2+}. Optimizing the NW growth process is essential to synthesize uniform-diameter NWs. Defects can occur when oxygen molecules are trapped in the lattice hexagonal structure of ZnO if the surrounding medium is not under sufficient vacuum in the hydrothermal process [17]. In addition, the presence of oxygen molecules can affect the electrical properties of the ZnO thin film due to a less-efficient electron transfer and the reduction of the electron mobility in the ZnO thin film [34]. The oxygen molecules also can decrease the quality of the ZnO crystals by reducing the lattice parameter "c" [35]. Therefore, the ZnO NW diameters can be optimized by annealing the synthesized ZnO thin film with different annealing times prior to the growth of the ZnO NWs. The morphology characteristics of the ZnO thin films, treated with different annealing times prior to ZnO NW synthesis, were investigated by X-ray diffraction (XRD) analysis.

3.4. XRD analysis

XRD analysis was carried out to investigate the phase and structure of the ZnO thin films prior to the growth of the ZnO NWs. Fig. 3 shows that all of the diffraction peaks matched well with the crystal structure of wurtzite ZnO. Peaks at 2θ values of 32.23°, 34.40°, 38.25°, 48.53°, 57.50° and 64.32° could be accurately indexed to the (100), (002), (101), (102), (110) and (103) crystal planes of ZnO crystallites, respectively (JCPDS no. 36-1451). In Fig. 3, the diffraction peaks of (002) are stronger than the other peaks, suggesting ZnO growth on the c-axis. The lattice constants "a" and "c" were calculated by the following formula:

$$a = \sqrt{\frac{1}{3}}\,\frac{\lambda}{sin\theta} \quad (3)$$

$$c = \frac{\lambda}{\sin\theta} \quad (4)$$

where λ is the X-ray wavelength of the incident CuK_α radiation (0.15 nm) and θ = 17.20. The lattice constants obtained were a = 3.004 Å and c = 5.207 Å. Hence, from the values obtained for the lattice constants "a" and "c", the growth axis directions of ZnO can be determined. Because the value of lattice constant "c" was more than that of lattice constant "a", the dominant growth orientation of ZnO was along the c-axis. This expected behavior can be correlated with the observation of the (002), (100) and (101) peaks having higher intensities than the (102), (110) and (103) peaks.

By applying the Debye–Scherer equation [36], the crystallite size of the wurtzite ZnO was 110 nm based on the most intense peak (002). This peak demonstrated that of the most highly crystalline wurtzite ZnO was formed oriented along the c-axis [37]. The formula for the Debye–Scherer equation is

$$D = \frac{\kappa\,\lambda}{FWHM\cos\theta} \quad (5)$$

where FWHM is the full width at half maximum, D is size of the crystallites, λ is the wavelength of Cukα radiation (0.1514 Å), and k is the correlation factor (0.94). With references to the JCPDS data (Powder Diffraction File, Card no: 36-1451), the XRD data show strong significance with the ZnO indexed to the wurtzite structure and convincingly validate that the ZnO NWs have been embedded with IDE electrodes for detecting low concentrations of glucose. To elucidate the crystalline properties of the ZnO thin film prior to the growth of the ZnO NWs, the ZnO thin film was annealed for different time periods, which are shown in Fig. 3.

The intensity of the peak at 34° increased with increasing annealing time from 1 to 5 h, indicating that the annealing had effectively transformed the amorphous structure of ZnO into a highly crystalline structure. This effect is illustrated by the increases in the crystallite sizes of the ZnO thin films with increasing annealing time. As the preferential peak of the ZnO thin films (002) increases with increasing annealing time, the most intense ZnO peak becomes narrower, showing that the crystalline properties of ZnO have improved significantly. Table 1 also reported that the crystalline grain size increased after undergoing the annealing process for 5 h, and the smallest diameter of the synthesized ZnO NWs was obtained, as illustrated in Fig. 2A. By referring to Scherrer's equation, the crystalline sizes of the ZnO thin film that underwent 1, 3 and 5 h of annealing were 50, 100 and 110 nm, respectively. High-quality crystalline ZnO thin films have greater tendencies to synthesize larger crystal grain sizes [38]. Hence, smaller nucleation sizes will synthesize smaller quasi-1D NWs that can be tailored to develop a sensitive biosensor.

3.5. UV–Vis analysis

UV–Vis spectroscopy measurements were carried out to evaluate the optical transparency of the ZnO thin films on quartz substrates. As shown by the transmission spectrum in Fig. 4A, the ZnO annealed for 1 h exhibited excellent transmittance, at approximately 98–100% in the visible wavelength ranging from 450 to 700 nm, compared to other regions. However, the transmittance was reduced as the annealing time increased from 1 to 5 h. The

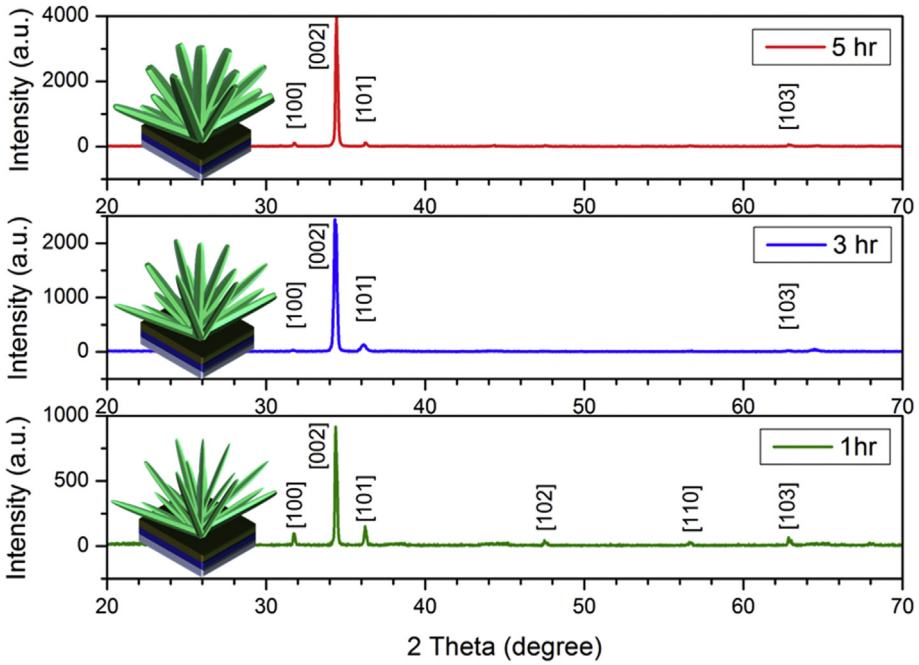

Fig. 3. Morphological characterization of the crystalline quality of the thin film treated for different annealing times. XRD analysis ($2\theta = 30^{\circ}-70^{\circ}$) of the as-synthesized ZnO thin film. The XRD patterns of the corresponding ZnO thin films annealed at 200 °C for 1, 3 and 5 h are shown.

Table 1
Structural properties of ZnO thin film prior to NWs formation.

Annealing time period	FWHM	D (nm)	a	c	L (A^0)
1 h	1.740×10^{-3}	50	3.22 Å	5.00 Å	1.77
3 h	1.396×10^{-3}	100	3.00 Å	5.21 Å	1.76
5 h	1.390×10^{-3}	110	3.00 Å	5.21 Å	1.76

spectrum illustrates that transmission occurred at a wavelength of 380 nm, which shows that ZnO is associated with highly crystalline properties, and the ZnO coated on the glass substrate was highly uniform and had less surface roughness [39]. A drastic change in the transmission of individual ZnO films treated for different annealing times is illustrated in Fig. 4A. As the samples were treated with longer annealing times, the transmission percentages of the samples decreased, showing a significant coherent increment of crystalline-sized ZnO thin film. The transmission spectrum of ZnO is strongly influenced by surface scattering and grain boundaries, which varies due to the annealing effect. To further validate the optical properties of the ZnO thin film, the band gap value was graphed using a Tauc plot by utilizing the following formula:

$$\alpha h\nu = B(h\nu - Eg)^n \tag{6}$$

where α represents the absorption coefficient, '*B*' is a constant, $h\nu$ represents the photon energy, Eg is the band gap energy and 'n' assumes the value of 1/2 for an allowed direct transition. The absorption coefficient, α, is obtained based on the following formula:

$$\alpha = \left(\frac{1}{d}\right) ln\left(\frac{(1-R)}{T}\right) \tag{7}$$

where 'd' represents the thickness, 'R' is the reflectance of ZnO, and 'T' is the transmission of ZnO [40]. Tauc plots of ZnO thin films with different annealing times are illustrated in Fig. 4C.

The band gap values of the ZnO thin films significantly decreased as they were treated with longer annealing processes at a constant temperature of 200 °C. The band gap values obtained from the ZnO thin films treated for 1, 3 and 5 h were 3.26 eV, 3.20 eV and 3.17 eV, respectively. A decreased band gap value indicates that the grain size of the ZnO crystals increased and also shows that the crystal grain growth in the annealed ZnO thin films increased [39]. Decreases in the effective band gap occurred as the crystal grain size increased because the absorption peak of the ZnO thin film increased with increasing annealing time (Fig. 4B). A quantum size effect also affects the value of the effective band gap energy based on the crystal grain size, which is explained based on the following formula:

$$E_{(\text{gap,nanocrystal})} = \mathrm{E}_{(\text{gap,bulk})} + \frac{\pi^2 \mathrm{h}^2}{2R^2}\left(\frac{1}{m_e} + \frac{1}{\mathrm{m}_h}\right) - 0.248\mathrm{E}_{\mathrm{Ry}} \tag{8}$$

where the ZnO bulk band gap, $\mathrm{E}_{(\text{gap, bulk})}$ value is 3.20 eV, and E_{Ry} is the bulk binding energy, which is 60 meV [41]. The electron and hole effective masses are taken as $m_e = 0.24m_o$ and $m_h = 2.31m_o$. In addition, 'h' represents the Planck constant, and 'R' is the radius of the crystal grain. To investigate the crystallinity level of ZnO, the Urbach energy, E_v was calculated based on the following formula:

$$\alpha = \alpha_0 \, exp\left(\frac{h\nu - \mathrm{E1}}{\mathrm{Ev}}\right) \tag{9}$$

According to Fig. 4D, the ZnO film that underwent a 1 h annealing treatment has the lowest value of the Urbach energy, E_v, followed by the ZnO films that underwent 3 and 5 h annealing treatments. The Urbach energy value increased with the duration of the annealing treatment. This result shows that the ZnO film that underwent the 1 h annealing had excellent structural properties due to its lowest Urbach energy values. Low Urbach energy values indicate minimal structural defects of the ZnO thin films [42]. After optimizing the ZnO thin films with various annealing times at a fixed temperature, the optimized ZnO thin film underwent

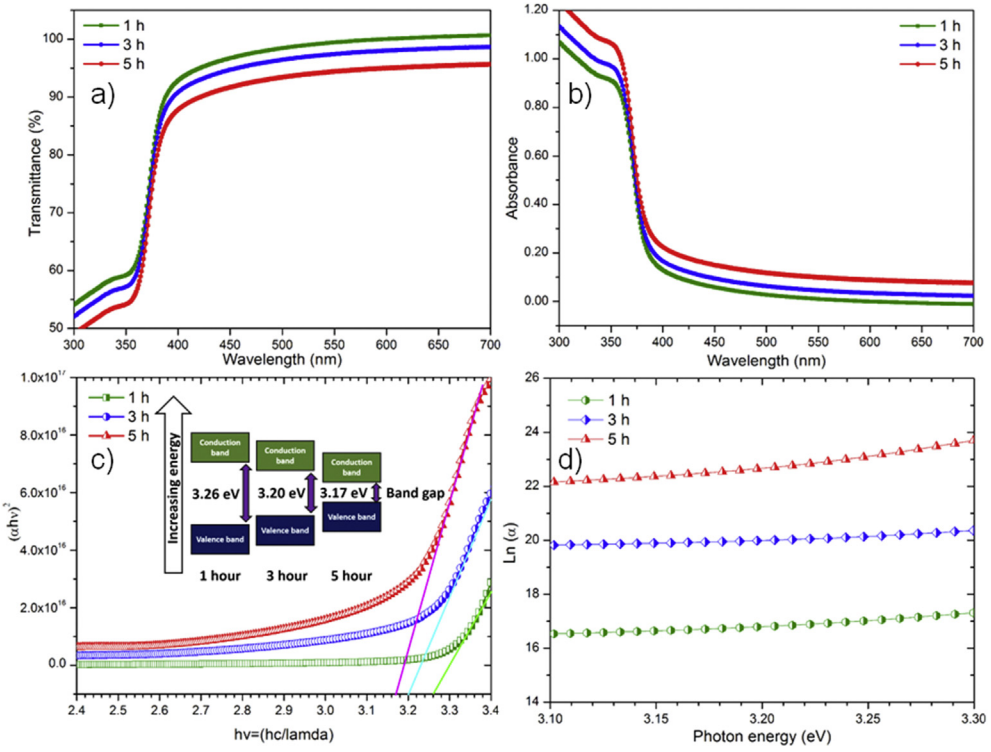

Fig. 4. Optical investigation of the transmission performances. (a) UV–Vis transmission and (b) absorption spectra of the ZnO thin film treated for different annealing times, (c) Band gap energy of ZnO thin films annealed for 1, 3 and 5 h. (d) Urbach plot graph of ZnO with different annealing time period.

hydrothermal growth to synthesize the ZnO NWs. The ZnO NW with the smallest diameter, 21 nm, was utilized to conduct surface functionalization for glucose detection at various concentrations. Electrical characterizations were conducted to validate the attachment of glucose oxidase (GOx) immobilized on the surface of the ZnO NWs because the selective enzyme specifically interacts with glucose.

3.6. Current vs voltage (I–V) and impedance measurements for surface chemical functionalization

Fig. 5 shows the I–V and impedance measurements of surface modified and non-surface modified interdigitated ZnO NW electrode for glucose detection. Based on the result in Fig. 5A and B, the current responds and impedance value have shown significant changes when the developed sensor was treated with surface modification on ZnO NW interface followed by the glucose solution. Changes in the current respond and impedance value for non-surface modified does not shows significant changes when interface was with glucose solution which indicated that chemical reaction between glucose solution and the surface of non-modified ZnO NW was not occur.

Fig. 6 illustrates the I–V and impedance measurements of the interdigitated high-performance ZnO NW modified electrode as a glucose biosensor, these measurements are essential for recognition of the surface functionalization on the ZnO NW for glucose detection. Initially, current versus voltage (I–V) and impedance tests were conducted before and after the surface chemical functionalization i.e. APTES (3-aminopropyltriethoxysilane) and after immobilization of GOx on the ZnO NW modified IDE, as shown in Fig. 6A and B. Fig. 6A clearly shows that the ZnO NWs has a forward current behavior in the range from 0 to 1.0 V. From the current-to-voltage relationship, it can be inferred that the device exhibited a linear relation between the current and voltage. Furthermore, it was observed that the bare ZnO NW IDE sensor showed a very low current to almost zero, due to high surface to volume ratio of ZnO NW consequently, causing oxygen molecules at an ambient atmosphere to react on the surface of ZnO NW, which eventually lead to adsorption of electron from conduction band of ZnO NW. Subsequently, electrical conductivity on the ZnO NW decreased, which attributes to an increase in the surface resistance of ZnO NW. However, a higher current of 1.7×10^{-6} A was measured at 0.95 V, when APTES was immobilized on the ZnO NWs, as shown in Fig. 6A. The electrical conductivity of the ZnO NWs increased after interfacing with APTES due to the reduced oxide group of ZnO, caused by the reaction with the ethoxyl group of aminosilane in anhydrous solvent and form amine functionalized group by the reaction shown below [43]:

$$\mathrm{ZnO{-}OH + C_2H_5{-}O{-}Si{-}X \longrightarrow ZnO{-}O{-}Si{-}X + C_2H_5OH} \quad (10)$$

where X is APTES 3-aminopropyltriethoxysilane $[H_2N(CH_2)_3(OC_2H_5)_2]$. When the APTES was introduced to ZnO surface, the silanization process results in the release of the electron back to the conduction band. This process causes an increase in electron density and decrease in the resistance which leads to rise in current. A significant current decreased approximately 72.96%, from 1.7×10^{-6} A to 1.07×10^{-6} A, at a fixed voltage supply of 0.95 V after immobilizing GOx as shown in Fig. 6A. This result indicates that GOx was immobilized successfully on the APTES-modified ZnO NWs.

AC impedance spectroscopy has been employed to elucidate the surface functionalization by APTES, immobilization of the GOx and glucose solution interface on the ZnO NWs. The sensing mechanism of changes in conduction (R) and polarization (C) at interfacial surface of glucose bio-electrode during the enzymatic reaction catalyzed by GOx process caused alteration in its impedance. Nyquist plot of the ZnO NW consists of grain (Rg), grain boundaries

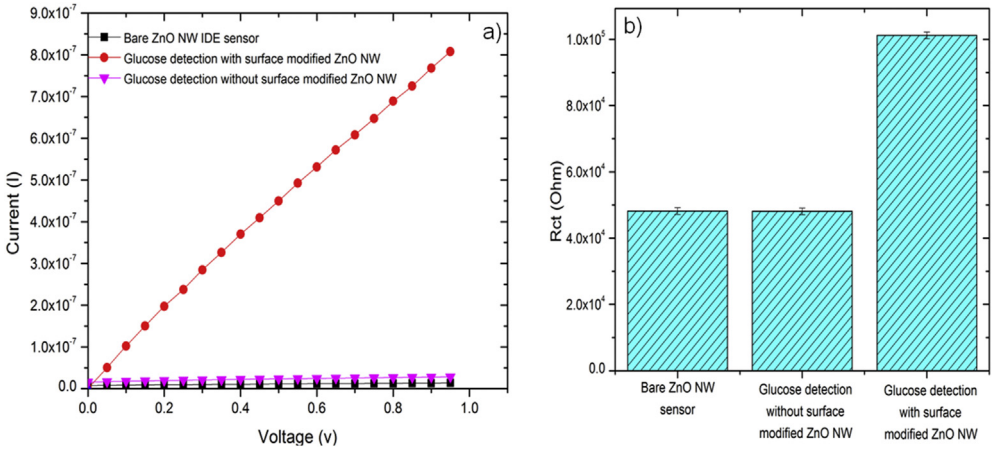

Fig. 5. Electrical characterization conducted on surface modified ZnO NWs and non-surface modified ZnO NWs for glucose detection. (a) Current-voltage (I–V) spectra and (b) Impedance measurement on the surface modified ZnO NWs and non-surface modified ZnO NWs for glucose detection.

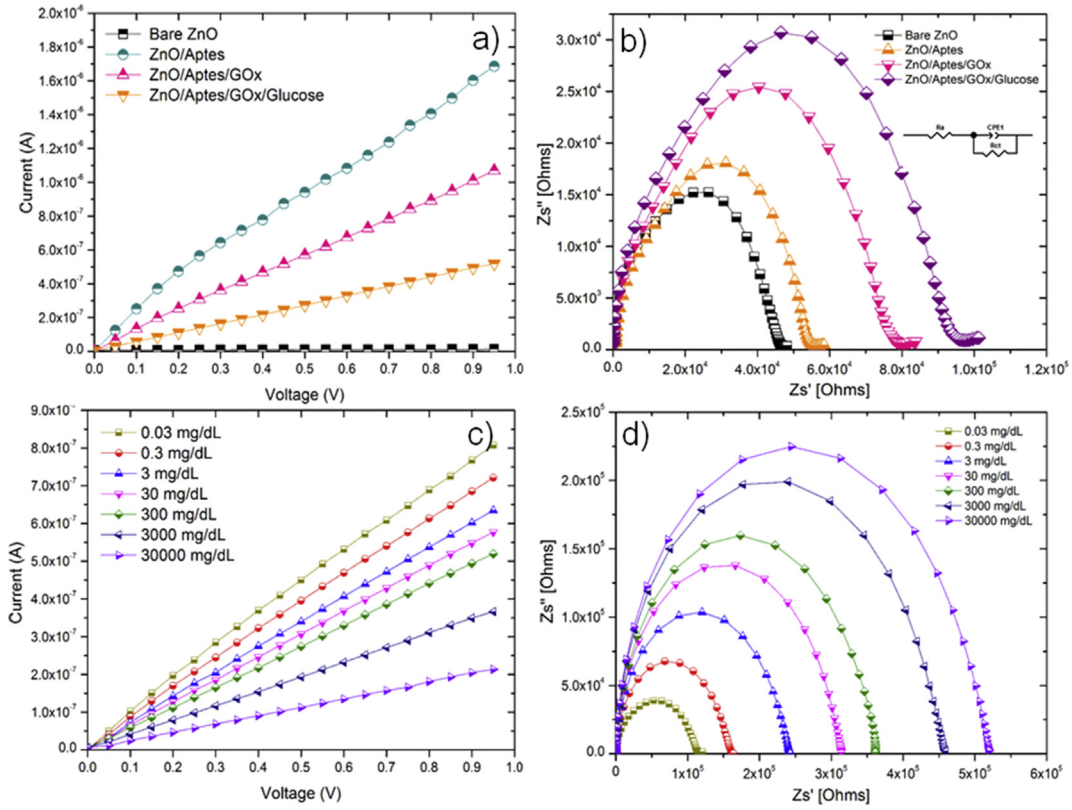

Fig. 6. Electrical characterization conducted with surface modification on the ZnO NWs with APTES attachment, GOx immobilization and dose-dependent glucose detection. (a) Current-voltage (I–V) spectra and (b) Impedance measurement of the surface modifications of the ZnO NWs with APTES attachment and GOx immobilization, (c) I–V measurement of glucose with concentration from 0.03 to 30,000 mg/dL and (d) Impedance measurement of glucose with concentrations from 0.03 to 30,000 mg/dL.

(Rgb, Cgb) and the IDE metal contact pad (Rc,Cc). Hence, the total impedance of ZnO NW can be obtained using the following equation:

$$Zt = Zg + Zgb + Zc \quad (11)$$

The obtained Nyquist plot can be expressed by Randles equivalent circuit (insert Fig. 6B), where the parameter Ra, Rct and CPE represents the resistance of bulk solution, charged transfer resistance and constant phase element, respectively. The semicircle in impedance spectra shown in Fig. 6B represents the interfacial charge transfer resistance, Rct corresponding to the carrier transfer from the modified electrode. From Fig. 6B it is noticeable that the interfacial Rct increased, when the surface of ZnO NW was modified by APTES, followed by GOx. The current and impedance behavior towards different concentrations of glucose was depicted in Fig. 6C and D, respectively. It showed a significant reduction in current response when the proposed sample detected increasing of glucose concentrations. In contrary, the charge transfer resistance, Rct of impedance spectra showed increasing Rct value with

increasing glucose concentrations from 0.03 to 30,000 mg/dL.

Glucose will undergo an enzymatic reaction catalyzed by GOx to form products and this mechanism can be described by the following equation [2,21]:

$$\text{Glucose} + O_2 + H_2O \xrightarrow{GO_x} \text{D} - \text{Glucona 1, 5 Lactone} + H_2O_2 \quad (12)$$

$$\text{D-Glucona 1,5 Lactone} \longrightarrow \text{gluconate}^- + H^+ \quad (13)$$

The enzymatic reaction of glucose with GOx will result to release D-glucona 1, 5 Lactone and hydrogen peroxide, and the oxygen consumption can be used for the glucose determination. The reaction of above product with H_20 will spontaneously produce gluconic acid with neutral pH. The gluconic acid and H+ are resulting from the above reaction will decrease the medium pH, which can be correlated to determined glucose concentration. The higher concentration of glucose, have the higher number of H^+ ion, which will increase the resistance, causing significant increase in charge transfer resistance, Rct [43]. Hence when the concentration of the glucose solution was reduced from 30,000–0.03 mg/dL, the product were reduced significantly and thus, enabling the reduction in Rct values.

3.7. Assessment of glucose in real blood sample

Measurements of glucose level in blood samples were conducted by using the commercial glucose meter and the developed ZnO NW IDE glucose sensor to validate the credibility of the proposed biosensor. Fig. 7A shows the reading of the blood glucose level from three samples. It showed that the glucose levels for three tested samples were low before meal intake and gradually increased after one hour of meal has taken. Subsequently, the glucose levels gradually reduced after two hours of their meal. This result shows a good agreement with the National Institute for Clinical Excellence (NICE) for non-diabetes samples. Fig. 7B shows AC impedance reading of blood glucose from the samples measured in parallel using the proposed ZnO NW IDE glucose sensor. From Fig. 7B, it was noted that the Rct values of all samples were low, which indicates low glucose level and the Rct values increased after one hour of meal taken, which shows an increment in glucose level. Furthermore, the Rct values of samples reduced after two hour of meal. Fig. 7C shows the charge transfer resistance correlation between glucose solution and real blood sample. The proposed ZnO NW IDE glucose sensor is able to detect blood glucose optimally in the range of 30–300 mg/dL. Therefore, the fabricated ZnO NW IDE glucose sensor can perform well, similar to the commercialized blood glucose meter.

3.8. Analytical performance of ZnO NW IDE glucose sensor

The staircase current-time response of the developed ZnO NW IDE glucose sensor is illustrated in Fig. 8A, describes the real-time detection at various glucose concentrations. For each injection (10 μL) of prepared concentrated glucose solution, three readings were measured continuously for 30 s to elucidate the performance of glucose sensor. Further injection of higher concentrations of glucose solution led to a significant reduction in current response and reached 95–97% of steady-state current within 3 s and obtained the saturation level. It clearly showed that the response time behavior of ZnO IDE glucose sensor with a wide range of glucose concentrations is comparatively better than the previous study reported in which longer response time was reported.

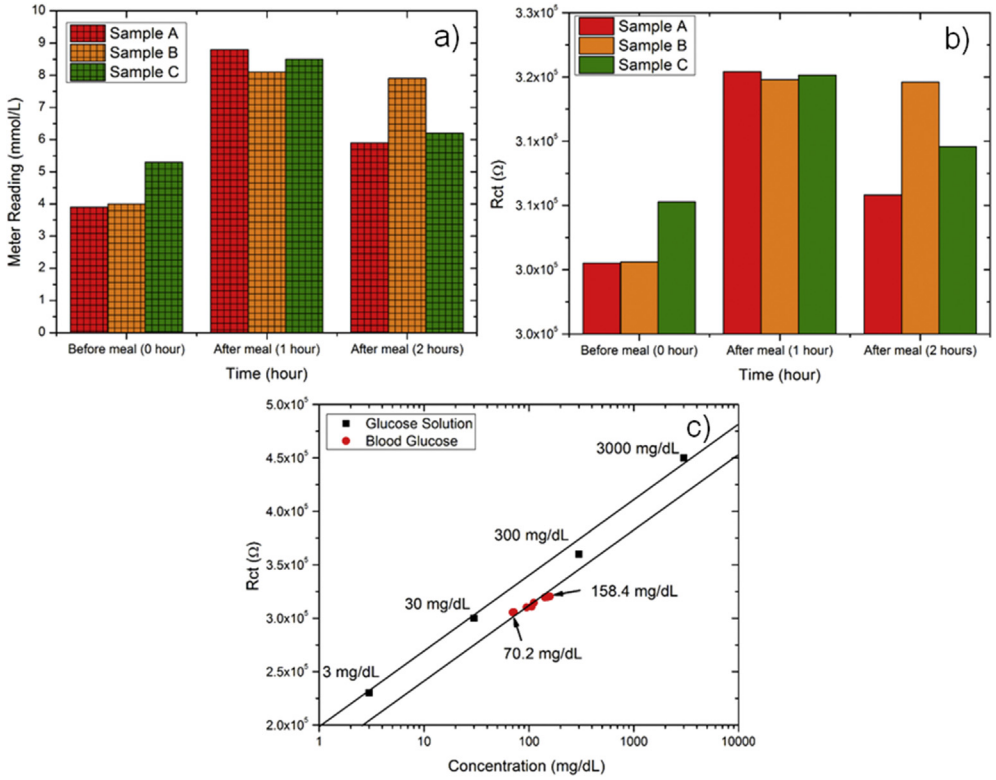

Fig. 7. Comparison measurement of glucose level in blood using commercial glucose meter and the developed ZnO NW IDE glucose sensor to validate the credibility of the proposed biosensor. (a) Reading of the blood glucose level before meal and after meal of 1 h and 2 h using commercial glucose meter, (b) Impedance measurement of yhr blood glucose level before meal and after meal of 1 h and 2 h and (c) Charge transfer resistance correlation between glucose solution and real blood sample.

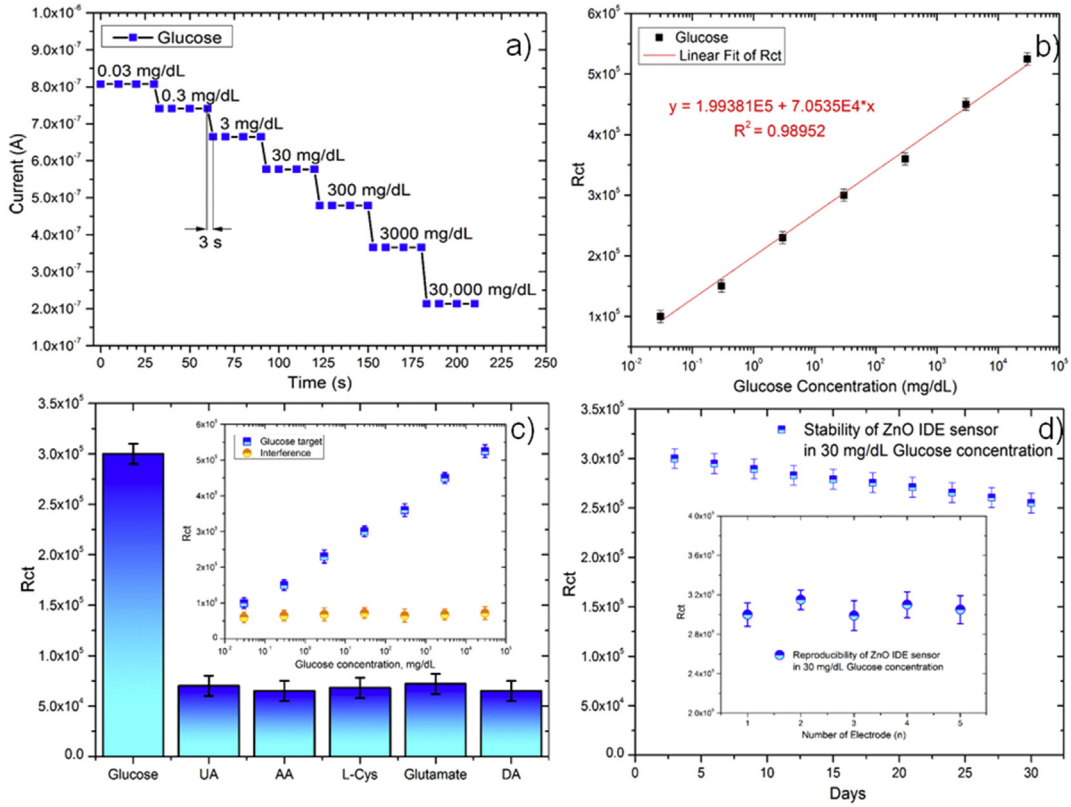

Fig. 8. Analytical performance of ZnO NW IDE glucose sensor. (a) The staircase current-time response of the developed ZnO NW IDE glucose sensor for real-time detection at various glucose concentrations. (b) Linearity plot with glucose concentrations ranging from 0.03 to 30,000 mg/dL, (c) Charge transfer resistance, (Rct), with uric acid (UA), ascorbic acid (AA), L-cysteine (l-cys), glutamate and dopamine acid (DA) and insert of Fig. 7C illustrates that the Rct value of the interference species in different concentration compared with glucose solution. (d) Stability of ZnO NW IDE sensor in 30 mg/dL glucose concentration.

The optimized performance of ZnO IDE glucose sensor was further validated via measuring the linearity plot with glucose concentrations ranging from 0.03 to 30,000 mg/dL which is depicted in Fig. 8B. The linear regression equation shown in Fig. 8B evidenced that ZnO IDE glucose sensor exhibit excellent linearity sensor behavior towards different glucose concentrations. The sensitivity of the sensor is measured by utilizing the following formula:

$$Sensitivity = \frac{Slope\ of\ calibration\ plot, m(\Omega\ \mathrm{mg}^{-1}\ \mu\mathrm{l})}{Active\ Surface\ Area,\ A(cm^2)} \quad (14)$$

The sensitivity of ZnO IDE glucose sensor is 28.56 Ω mg^{-1} μl on the platform active sensing area, A = 0.00900 cm^2. The limit of detection, LOD of ZnO IDE glucose sensor is 0.03 mg/dL which was calculated by signal to noise ratio of 3σ (where σ represents standard deviation of the blank solution, n = 5). Although the detection limit of the sensor is limited to 0.03 mg/dL, lower concentration of glucose could also be recognized, which shows its superior performance.

Evaluating the selectivity of ZnO IDE glucose sensor is mandatory to ensure that this sensor only specifically recognize the presence of glucose. It is known that human blood serum contains common interfering species, such as uric acid (UA), ascorbic acid (AA), L-cysteine (l-cys), glutamate and dopamine acid (DA). Hence, the anti-interference ability of the sensor was tested by injecting the stated interfering species. Fig. 8C shows that the charge transfer resistance, (Rct), with uric acid (UA), ascorbic acid (AA), L-cysteine (l-cys), glutamate and dopamine acid (DA) were not significantly changed. Further, insert Fig. 8C illustrates that the Rct value of the interference species in different concentration compared with glucose solution. It was observed that the value of Rct signal does not vary significantly in the presence of unrelated molecules indicating non-influence of the individual interferants. This shows that the sensor has specifically recognize the presence of glucose and hence it is evidenced that ZnO IDE glucose sensor is tailored for detecting the glucose level in real blood samples.

Stability performance of the proposed ZnO IDE glucose sensor was validated by the shelf-life study for a period of 30 days, examined with three days intervals and the sensor was stored at temperature 4 °C. Based on the results displayed in Fig. 8D, the stability of the device is sufficient and only loss 10% of its activity after 30 days period of time. Superior stability of the IDE glucose sensor has attributed that ZnO NW has bio-compatibility with GOx and does not inhibit GOx activity. However, the 10% deterioration over the period of 30 days may be caused by denaturation of GOx activity and it can be improved by optimizing the packaging method of the glucose sensor. Insert of Fig. 8D shows the Rct error bar value of five IDE sensors, which was prepared under similar processing condition. The calculated relative standard deviation (R.S.D) of 5% with repetition of 5 sensors significantly shows promising reproducibility of the developed ZnO IDE glucose sensor.

Table 2 illustrates the comparative sensor performances of the proposed Interdigitated ZnO nanowire (NW) modified electrode glucose sensor with other glucose sensor. Based on the data obtained (Table 2), it is clearly shown that the current work have superior performances compared to previous reports. The proposed glucose sensor exhibits excellent sensing performances with low limit of detection down to 1.665 μM (0.03 mg/dL) with fast respond time (3s) to be suitable for wide range glucose detection.

Table 2
Comparison of proposed ZnO NW-modified IDE glucose biosensor with previously developed glucose biosensors.

ZnO nanostructure	Ligand	Analyte	Limit of detection (mg/dL)	Respond time	Reference
ZnO–Co nanocluster	GoX	Glucose	0.36	8 s	[44]
Tetragonal pyramids ZnO nanostructure	GoX	Glucose	0.18	Less than 5 s	[45]
ZnO NF	GoX	Glucose	0.02	4 s	[46]
ZnO Tetrapod	GoX	Glucose	0.07	6 s	[47]
ZnO NR	GoX	Glucose	0.05	5 s	[48]
Porous ZnO nanostructure	GoX	Glucose	0.18	7 s	[49]
ZnO NW modified IDE biosensor	GoX	Glucose	0.03	3 s	Present work

The dimensional size of the proposed IDE electrode is 0.5 × 0.8 cm which is smaller compared to the test strips of the conventional glucose sensor. The cost of fabricating the sensor is economical due to less complex operating procedure and the route to fabricate IDE sensor does not involve critical procedure and costly equipment. Considering the material laboratory, the overall cost of our sensor is comparatively negligible. Only preparation of 'Mask' needs standard cost. One of the main highlighted advantages of the developed ZnO NW-modified Interdigitated electrode (IDE) sensor is the device can be reusable after undergoing cleaning procedure compared to the conventional glucose test stripes, which cannot be used again. Based on the morphological and electrical result of the annealed ZnO NW, it is proved that ZnO NW with the thin film was treated for 1 h of annealing time period showed excellent crystalline properties which is tailored for glucose sensing.

4. Conclusions

Herein, we have demonstrated a new fabricated ZnO NW-modified IDE electrochemical glucose biosensor. It was found that the crystallite size of the ZnO thin film increases with increasing annealing time. The size of the smallest synthesized ZnO NW was approximately 21 nm. The performance of this biosensor was investigated through interactions with GOx and glucose in a dose-dependent manner. Smaller ZnO NWs facilitate the proper immobilization of APTES and the consequent interaction of GOx with glucose at a low concentration (30 mg/dL) with the fastest steady-state response time of 3 s. Assessment with real blood samples and comparative studies using commercial glucose meter, yielded further support to ZnO NW-modified IDE sensor. The performance of the ZnO NW-modified IDE was comparatively better than the performances of other sensors that were generated based on different ZnO nanostructures. The sensor fabricated here, which is fast and has a low detection limit, an option for a new class of glucose biosensor.

Acknowledgments

Authors gratefully acknowledge collaborators at the Institute of Nano Electronic Engineering (INEE), University Malaysia Perlis (UniMAP) and Ministry of Higher Education Malaysia for the financial support through MTUN-COE grant 9016-00004 for giving the opportunities to conduct the research in the Biochip Lab, Failure analysis lab and Microfabrication cleanroom. This project was also aided by INEE (UniMAP) through the Nano Technology project.

References

[1] V. Baldo, S. Lombardi, S. Cocchio, S. Rancan, A. Buja, S. Cozza, et al., Diabetes outcomes within integrated healthcare management programs, Prim. Care Diabetes 9 (2015) 54–59, http://dx.doi.org/10.1016/j.pcd.2014.03.005.
[2] Y. Zhai, S. Zhai, G. Chen, K. Zhang, Q. Yue, L. Wang, et al., Effects of morphology of nanostructured ZnO on direct electrochemistry and biosensing properties of glucose oxidase, J. Electroanal. Chem. 656 (2011) 198–205, http://dx.doi.org/10.1016/j.jelechem.2010.11.020.
[3] M.-L. Ho, J.-C. Wang, T.-Y. Wang, C.-Y. Lin, J.F. Zhu, Y.-A. Chen, et al., The construction of glucose biosensor based on crystalline iridium(III)-containing coordination polymers with fiber-optic detection, Sens. Actuators B Chem. 190 (2014) 479–485, http://dx.doi.org/10.1016/j.snb.2013.08.100.
[4] J. Luo, P. Luo, M. Xie, K. Du, B. Zhao, F. Pan, et al., A new type of glucose biosensor based on surface acoustic wave resonator using Mn-doped ZnO multilayer structure, Biosens. Bioelectron. 49 (2013) 512–518, http://dx.doi.org/10.1016/j.bios.2013.05.021.
[5] Y.-M. Sung, K. Noh, W.-C. Kwak, T.G. Kim, Enhanced glucose detection using enzyme-immobilized ZnO/ZnS core/sheath nanowires, Sens. Actuator B Chem. 161 (2012) 453–459, http://dx.doi.org/10.1016/j.snb.2011.10.061.
[6] J.Y. Kim, S.-Y. Jo, G.-J. Sun, A. Katoch, S.-W. Choi, S.S. Kim, Tailoring the surface area of ZnO nanorods for improved performance in glucose sensors, Sens. Actuators B Chem. 192 (2014) 216–220, http://dx.doi.org/10.1016/j.snb.2013.10.113.
[7] P. Yang, L. Wang, Q. Wu, Z. Chen, X. Lin, A method for determination of glucose by an amperometric bienzyme biosensor based on silver nanocubes modified Au electrode, Sens. Actuators B Chem. 194 (2013) 71–78, http://dx.doi.org/10.1016/j.snb.2013.12.074.
[8] K.-Y. Ahn, K. Kwon, J. Huh, G.T. Kim, E.B. Lee, D. Park, et al., A sensitive diagnostic assay of rheumatoid arthritis using three-dimensional ZnO nanorod structure, Biosens. Bioelectron. 28 (2011) 378–385, http://dx.doi.org/10.1016/j.bios.2011.07.052.
[9] S.R. Balakrishnan, U. Hashim, G.R. Letchumanan, M. Kashif, A.R. Ruslinda, W.W. Liu, et al., Development of highly sensitive polysilicon nanogap with APTES/GOx based lab-on-chip biosensor to determine low levels of salivary glucose, Sens. Actuators A Phys. 220 (2014) 101–111.
[10] J.-H. Kim, B.-M. Moon, S.-M. Hong, Capacitive humidity sensors based on a newly designed interdigitated electrode structure, Microsyst. Technol. 18 (2011) 31–35, http://dx.doi.org/10.1007/s00542-011-1373-0.
[11] A. Choi, K. Kim, H.-I. Jung, S.Y. Lee, ZnO nanowire biosensors for detection of biomolecular interactions in enhancement mode, Sens. Actuators B Chem. 148 (2010) 577–582, http://dx.doi.org/10.1016/j.snb.2010.04.049.
[12] M.A. Chougule, S.L. Patil, S.G. Pawar, V.B. Patil, Scholars Res. Libr. 1 (2010) 100–107.
[13] M. Kashif, Y. Al-Douri, U. Hashim, M.E. Ali, S.M.U. Ali, M. Willander, Characterisation, analysis and optical properties of nanostructure ZnO using the sol–gel method, Micro Nano Lett. 7 (2012) 163, http://dx.doi.org/10.1049/mnl.2011.0681.
[14] M. Kashif, M.E. Ali, S.M.U. Ali, U. Hashim, S.B.A. Hamid, Impact of hydrogen concentrations on the impedance spectroscopic behavior of Pd-sensitized ZnO nanorods, Nanoscale Res. Lett. 8 (2013) 68, http://dx.doi.org/10.1186/1556-276X-8-68.
[15] V. Perumal, U. Hashim, S.C.B. Gopinath, R. Haarindraprasad, W.-W. Liu, P. Poopalan, et al., Thickness dependent nanostructural, morphological, optical and impedometric analyses of zinc oxide-gold hybrids: nanoparticle to thin film, PLoS One 10 (2015) e0144964, http://dx.doi.org/10.1371/journal.pone.0144964.
[16] V. Perumal, U. Hashim, S.C.B. Gopinath, H. Rajintra Prasad, L. Wei-Wen, S.R. Balakrishnan, et al., Characterization of gold-sputtered zinc oxide nanorods—a potential hybrid material, Nanoscale Res. Lett. 11 (2016) 1–11, http://dx.doi.org/10.1186/s11671-016-1245-8.
[17] A. Janotti, C.G. Van de Walle, Fundamentals of zinc oxide as a semiconductor, Rep. Prog. Phys. 72 (2009) 126501, http://dx.doi.org/10.1088/0034-4885/72/12/126501.
[18] K.L. Foo, M. Kashif, U. Hashim, M.E. Ali, Sol–gel derived ZnO nanoparticulate films for ultraviolet photodetector (UV) applications, Opt. Int. J. Light Electron Opt. 124 (2013) 5373–5376, http://dx.doi.org/10.1016/j.ijleo.2013.03.120.
[19] V. Perumal, U. Hashim, S.C.B. Gopinath, R. Haarindraprasad, K.L. Foo, S.R. Balakrishnan, et al., "Spotted nanoflowers": gold-seeded zinc oxide nanohybrid for selective bio-capture, Sci. Rep. 5 (2015) 12231, http://dx.doi.org/10.1038/srep12231.
[20] V. Perumal, U. Hashim, S.C.B. Gopinath, R. Haarindraprasad, P. Poopalan, W.-W. Liu, et al., A new nano-worm structure from gold-nanoparticle mediated random curving of zinc oxide nanorods, Biosens. Bioelectron. 78 (2016) 14–22, http://dx.doi.org/10.1016/j.bios.2015.10.083.
[21] N.K. Sarkar, S.K. Bhattacharyya, High electro-catalytic activities of glucose oxidase embedded one-dimensional ZnO nanostructures, Nanotechnology 24 (2013) 225502, http://dx.doi.org/10.1088/0957-4484/24/22/225502.
[22] R. Haarindraprasad, U. Hashim, S.C.B. Gopinath, M. Kashif, P. Veeradasan,

S.R. Balakrishnan, et al., Low temperature annealed zinc oxide nanostructured thin film-based transducers: characterization for sensing applications, PLoS One 10 (2015) e0132755, http://dx.doi.org/10.1371/journal.pone.0132755.
[23] R. Niepelt, U.C. Schröder, J. Sommerfeld, I. Slowik, B. Rudolph, R. Möller, et al., Biofunctionalization of zinc oxide nanowires for DNA sensory applications, Nanoscale Res. Lett. 6 (2011) 511, http://dx.doi.org/10.1186/1556-276X-6-511.
[24] R.H. Prasad, U. Hashim, Original articles a review on the label free nanowire based biosensor, J. Appl. Sci. Res. 8 (2012) 4759–4769.
[25] L. Cao, J. Jiang, L. Zhu, Realization of band-gap engineering of ZnO thin films via Ca alloying, Mater. Lett. 100 (2013) 201–203, http://dx.doi.org/10.1016/j.matlet.2013.03.031.
[26] Q. Humayun, M. Kashif, U. Hashim, Area-selective ZnO thin film deposition on variable microgap electrodes and their impact on UV sensing, J. Nanomater. 2013 (2013) 1–5, http://dx.doi.org/10.1155/2013/301674.
[27] N. Shakti, Struct. Opt. Prop. Sol gel Prep. ZnO Thin Film 2 (2010) 19–28.
[28] V. Kumar, N. Singh, R.M. Mehra, A. Kapoor, L.P. Purohit, H.C. Swart, Role of film thickness on the properties of ZnO thin films grown by sol-gel method, Thin Solid Films 539 (2013) 161–165, http://dx.doi.org/10.1016/j.tsf.2013.05.088.
[29] N.J. Kidner, Z.J. Homrighaus, T.O. Mason, E.J. Garboczi, Modeling interdigital electrode structures for the dielectric characterization of electroceramic thin films, Thin Solid Films 496 (2006) 539–545, http://dx.doi.org/10.1016/j.tsf.2005.08.350.
[30] Y.-T. Chang, J.-H. Huang, M.-C. Tu, P. Chang, T.-R. Yew, Flexible direct-growth CNT biosensors, Biosens. Bioelectron. 41 (2013) 898–902, http://dx.doi.org/10.1016/j.bios.2012.09.049.
[31] K. Khun, Z.H. Ibupoto, C.O. Chey, J. Lu, O. Nur, M. Willander, Comparative study of ZnO nanorods and thin films for chemical and biosensing applications and the development of ZnO nanorods based potentiometric strontium ion sensor, Appl. Surf. Sci. 268 (2013) 37–43, http://dx.doi.org/10.1016/j.apsusc.2012.11.141.
[32] C.L. Xu, L. Fang, F. Wu, Q.L. Huang, B. Yin, Wetting behavior of triethoxyoctylsilane modified ZnO nanowire films, Colloids Surfaces A Physicochem. Eng. Asp. 444 (2013) 48–53, http://dx.doi.org/10.1016/j.colsurfa.2013.12.025.
[33] A. Simimol, P. Chowdhury, S.K. Ghosh, H.C. Barshilia, Optimization of parameters for the growth of defect free ZnO nanorod arrays with intense UV emission capacity by electrochemcial route, Electrochim. Acta 90 (2013) 514–523, http://dx.doi.org/10.1016/j.electacta.2012.12.051.
[34] S.-K. Tzeng, M.-H. Hon, I.-C. Leu, Suppressing the atmosphere-induced performance instability of solution-grown zinc oxide-nanowire ultra-violet photodetector by hydrothermal treatment in water, Mater. Chem. Phys. 139 (2013) 963–967, http://dx.doi.org/10.1016/j.matchemphys.2013.02.062.
[35] X. Li, Y. Wang, W. Liu, G. Jiang, C. Zhu, Study of oxygen vacancies' influence on the lattice parameter in ZnO thin film, Mater. Lett. 85 (2012) 25–28, http://dx.doi.org/10.1016/j.matlet.2012.06.107.
[36] S. Benramache, B. Benhaoua, F. Chabane, A. Guettaf, A comparative study on the nanocrystalline ZnO thin films prepared by ultrasonic spray and solgel method, Opt. Int. J. Light Electron Opt. 124 (2013) 3221–3224, http://dx.doi.org/10.1016/j.ijleo.2012.10.001.
[37] K.L. Foo, M. Kashif, U. Hashim, W.-W. Liu, Effect of different solvents on the structural and optical properties of zinc oxide thin films for optoelectronic applications, Ceram. Int. 40 (2014) 753–761, http://dx.doi.org/10.1016/j.ceramint.2013.06.065.
[38] J. Zhang, W. Que, Preparation and characterization of sol–gel Al-doped ZnO thin films and ZnO nanowire arrays grown on Al-doped ZnO seed layer by hydrothermal method, Sol. Energy Mater. Sol. Cells 94 (2010) 2181–2186, http://dx.doi.org/10.1016/j.solmat.2010.07.009.
[39] K.K. Nagaraja, S. Pramodini, P. Poornesh, H.S. Nagaraja, Effect of annealing on the structural and nonlinear optical properties of ZnO thin films under cw regime, J. Phys. D. Appl. Phys. 46 (2013) 055106, http://dx.doi.org/10.1088/0022-3727/46/5/055106.
[40] A.I. Ali, A.H. Ammar, A. Abdel Moez, Influence of substrate temperature on structural, optical properties and dielectric results of nano- ZnO thin films prepared by radio frequency technique, Superlattices Microstruct. 65 (2014) 285–298, http://dx.doi.org/10.1016/j.spmi.2013.11.007.
[41] S. Singh, P. Chakrabarti, Comparison of the structural and optical properties of ZnO thin films deposited by three different methods for optoelectronic applications, Superlattices Microstruct. 64 (2013) 283–293, http://dx.doi.org/10.1016/j.spmi.2013.09.031.
[42] A.M. El Sayed, S. Taha, G. Said, F. Yakuphanoglu, Controlling the structural and optical properties of nanostructured ZnO thin films by cadmium content, Superlattices Microstruct. 65 (2014) 35–47, http://dx.doi.org/10.1016/j.spmi.2013.10.041.
[43] H. Deng, A.K.L. Teo, Z. Gao, An interference-free glucose biosensor based on a novel low potential redox polymer mediator, Sens. Actuators B Chem. 191 (2014) 522–528, http://dx.doi.org/10.1016/j.snb.2013.10.059.
[44] Z.W. Zhao, X.J. Chen, B.K. Tay, J.S. Chen, Z.J. Han, K.A. Khor, A novel amperometric biosensor based on ZnO: Co nanoclusters for biosensing glucose, Biosens. Bioelectron. 23 (2007) 135–139, http://dx.doi.org/10.1016/j.bios.2007.03.014.
[45] Z. Dai, G. Shao, J. Hong, J. Bao, J. Shen, Immobilization and direct electrochemistry of glucose oxidase on a tetragonal pyramid-shaped porous ZnO nanostructure for a glucose biosensor, Biosens. Bioelectron. 24 (2009) 1286–1291, http://dx.doi.org/10.1016/j.bios.2008.07.047.
[46] M. Ahmad, C. Pan, Z. Luo, J. Zhu, A single ZnO nanofiber-based highly sensitive amperometric glucose biosensor, J. Phys. Chem. C 114 (2010) 9308–9313, http://dx.doi.org/10.1021/jp102505g.
[47] Y. Lei, X. Yan, N. Luo, Y. Song, Y. Zhang, ZnO nanotetrapod network as the adsorption layer for the improvement of glucose detection via multiterminal electron-exchange, Colloids Surfaces A Physicochem. Eng. Asp. 361 (2010) 169–173, http://dx.doi.org/10.1016/j.colsurfa.2010.03.029.
[48] X. Liu, Q. Hu, Q. Wu, W. Zhang, Z. Fang, Q. Xie, Aligned ZnO nanorods: a useful film to fabricate amperometric glucose biosensor, Colloids Surfaces B Biointerfaces 74 (2009) 154–158, http://dx.doi.org/10.1016/j.colsurfb.2009.07.011.
[49] H. Fatemi, A.A. Khodadadi, A. Anaraki Firooz, Y. Mortazavi, Apple – biomorphic synthesis of porous ZnO nanostructures for glucose direct electrochemical biosensor, Curr. Appl. Phys. 12 (2012) 1033–1038, http://dx.doi.org/10.1016/j.cap.2012.01.001.